https://doi.org/10.1595/205651322X16529612227119 *Johnson Matthey Technol. Rev.*, 2022, **66**, (4), 393–405

JOHNSON MATTHEY
TECHNOLOGY REVIEW
technology.matthey.com

Development of New Mixed-Metal Ruthenium and Iridium Oxides as Electrocatalysts for Oxygen Evolution: Part I

Survey of crystal structures and synthesis methods

Jasmine A. Clayton, Richard I. Walton*
Department of Chemistry, University of Warwick, Gibbet Hill Road, Coventry, CV4 7AL, UK

***Email:** r.i.walton@warwick.ac.uk

PEER REVIEWED

Received 19th January 2022; Revised 4th May 2022; Accepted 19th May 2022; Online 19th May 2022

We review recent research into oxides of platinum group metals (pgms), in particular those of ruthenium and iridium, for use as electrocatalysts for the oxygen evolution reaction (OER). These are used in membrane electrode assemblies (MEAs) in devices such as electrolysers, for water splitting to generate hydrogen as fuel, and in fuel cells where they provide a buffer against carbon corrosion. In these situations, proton exchange membrane (PEM) layers are used, and highly acid-resilient electrocatalyst materials are required. The range of structure types investigated includes perovskites, pyrochlores and hexagonal perovskite-like phases, where the pgm is partnered by base metals in complex chemical compositions. The role of chemical synthesis in the discovery of new oxide compositions is emphasised, particularly to yield powders for processing into MEAs. Part I introduces the electrocatalytic splitting of water to oxygen and hydrogen and provides a survey of ruthenium and iridium oxide structures for oxygen evolution reaction catalysis.

1. Introduction

A key process in developing future devices for various energy-related applications is the electrocatalytic splitting of water to oxygen and hydrogen, and this is highly relevant for the sustainable and clean production of electricity or fuels in the move away from carbon-focused technologies. In an electrolyser, the anodic OER is a major limiting step in improving efficiency since it inherently possesses unfavourable thermodynamics, being a four-electron transfer reaction (1, 2). This leads to high overpotentials to drive the reaction, giving unfavourable kinetics, and can lead to energy losses within any electrochemical device. The activation barrier of the OER is much larger than that of the hydrogen evolution reaction (HER) at the cathode, and thus much attention is focused on discovery of electrocatalysts to overcome this barrier in order to optimise device performance. The two relevant half-equations in acid conditions can be represented in Equation (i) and Equation (ii):

HER at cathode:

$$4H^+ + 4e^- \rightarrow 2H_2 \quad E^0 = 0\ V \qquad (i)$$

OER at anode:

$$2H_2O(l) \rightarrow O_2(g) + 4H^+ + 4e^- \quad E^0 = 1.23\ V \qquad (ii)$$

OER in aqueous acid electrolytes is desirable since it provides high current densities and high voltage efficiency, and the fast kinetics of the partnering HER are beneficial (3, 4). Furthermore, contamination by aerial carbon dioxide and

precipitation of carbonates is avoided, which is not the case for alkaline electrolytes. The benefits of acid electrolysis are exploited in PEM devices that make use of proton-conducting polymer electrolytes, that are typically fluorocarbon or hydrocarbon polymers with sulfonic-acid side chains to provide transport of protons (5), and these polymers have been optimised over many years to give a well-developed technology (6). The PEM permits high gas purity and a compact system design in which gas crossover is low, and these are further significant advantages over alkaline devices (7). As well as obvious uses in water splitting to produce gases for fuels, an OER electrocatalyst is also of benefit in PEM fuel cells where it can be used to limit the carbon corrosion reaction that may occur under conditions of fuel starvation or with other excursions to high electrode potentials, instead evolving oxygen (8–10). This application thus mitigates against fuel cell degradation and prolongs their life. Electrocatalytic oxygen evolution is also closely associated with the charging process in metal–air batteries (11), and so understanding and optimising the OER is of key importance in this respect. With the rapidly growing demand, and indeed expectation, for efficient energy conversion and storage devices it is evident that electrocatalysis of the OER reaction is a crucial bottleneck to overcome.

While it is clear that acid-resilient electrocatalysts are in high demand to meet these applications, it is unfortunate that most metal oxide materials that might be candidate electrocatalysts are unstable at low pH and readily dissolve. While many oxides of many metals have been studied for OER electrocatalysis under alkaline conditions (12), presently the most promising materials for the acid conditions of PEM devices are oxides of pgms, in particular those of ruthenium and iridium (13–15). The binary dioxides RuO_2 and IrO_2 and solid-solutions thereof can be considered benchmark materials in this respect (16–20). These materials share the rutile-type structure, as would be found for the thermodynamically stable form of TiO_2, consisting of octahedrally coordinated tetravalent cations that share corners and edges to yield a three-dimensionally extended structure, **Figure 1**.

A tremendous amount of work has been focused on IrO_2-based materials, prepared by various synthesis routes, as both films and powders (21, 22). Nanocrystalline forms have been developed, which may permit surface reactivity to be tuned, as well as allowing processing for device fabrication (22–24). Many iridium oxide materials studied for electrocatalytic OER are poorly crystalline, or indeed amorphous to X-rays, and often the active phase is proposed to be a hydrous iridium oxide (25, 26). Examination of local atomic order of these poorly crystalline materials has identified structural motifs that are favourable for high electrocatalytic activity and that minimise dissolution of the solid under operating conditions; interestingly the rutile-like structure may be more prone to collapse than more open IrO_x structures (27). The phase IrO_3 has also been isolated *via* an ion-exchange process from β-Li_2IrO_3, *via* a protonated intermediate (28). Insertion of lithium into IrO_2 forms an amorphous phase with increased activity over crystalline IrO_2, with the structural flexibility of the amorphous structure proposed to enhance turnover of OER (29).

Partial substitution of iridium by non-pgms in IrO_2 has been extensively studied, with the aim of not only diluting the pgm content but also tuning activity and stability. For example, isovalent replacement of Ir^{4+} by Ti^{4+} (30, 31) or by Sn^{4+} (32, 33) has yielded materials with improved stability over pure IrO_2, although it may be noted that some of these materials actually consist of small particles

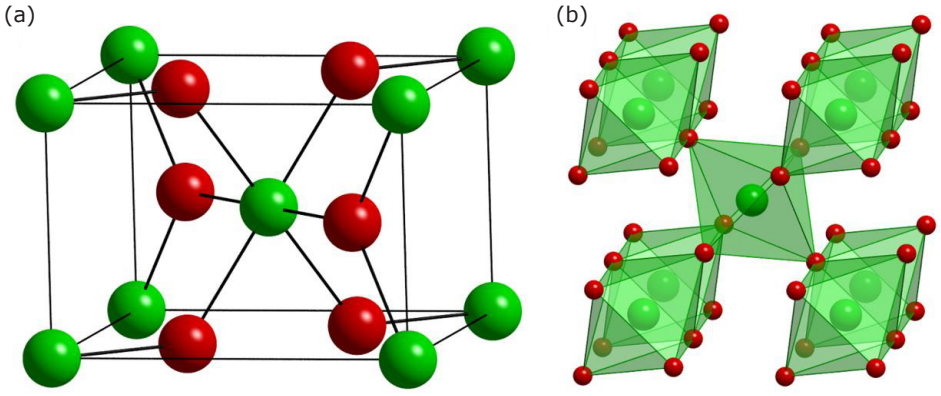

Fig. 1. The rutile structure as found for IrO_2 and RuO_2 shown as: (a) ball-and-stick view of tetragonal unit cell; and (b) a polyhedral representations showing corner- and edge-shared connectivity. Green spheres are iridium and red are oxygen

of IrO_2 supported on the second oxide (31). In other cases, a substituent cation may adjust the oxidation state of iridium to modify electrocatalytic properties: for example, inclusion of manganese was found to give a higher concentration of surface Ir^{3+} (34). Similar chemistry has been developed for RuO_2, which although suffers from lower stability than IrO_2 in acid electrolytes (35), partial elemental substitution by a variety of elements has proved possible, including various aliovalent first-row transition-metal cations (manganese, cobalt, nickel or copper) that introduce defects, or modify the average oxidation state of ruthenium (36–43). Addition of these as dopants at the surface of RuO_2 can have specific benefits: for example, adding nickel or cobalt enhances activity, which was rationalised computationally as from activation of a proton donor–acceptor functionality on conventionally inactive bridge surface sites (44). Combinations of two substituent elements introduce further tunability to these systems, such as strontium-ruthenium-iridium oxides (45), or cerium-ruthenium-iridium oxides (46). Such complex solid solutions must be carefully structurally characterised, since local segregation of the metals may occur, to give preferential surface enrichment of one (17, 47), although if carefully engineered this can lead to enhanced properties (48, 49).

Although precious-metal-free materials may be desirable for economic reasons (50), and indeed some manganese oxides have recently been suggested as alternatives that have been claimed to operate over a range of pH (51, 52), iridium and ruthenium oxides remain the most active and robust materials for OER under acidic conditions. One strategy to overcome the use of expensive and limited pgms is to use complex ternary oxides with the precious metal diluted by the presence of a non-precious metal. Goodenough and coworkers made the first investigations of such materials, with a study in 1990 of the electrocatalytic properties of pyrochlores $Pb_2(Ir_{2-x}Pb_x)O_{7-y}$ and $Pb_2(Ru_{2-x}Pb_x)O_{7-y}$ as a function of pH (53). This was followed by work in 1995 by ten Kortenaar *et al.* who studied a range of ternary iridium oxides for their activity towards OER (54), and although they found no correlation between crystal structure and activity, they discovered some materials with promising properties including those with pyrochlore and fluorite structures (see Section 2). With the resurgence of interest in electrocatalysts for OER, recent work in the past five years has focused on discovery of new acid-stable and highly active ruthenium and iridium oxides with an emphasis on thrifting of precious metals (55). This includes multi-element oxides so that the pgm is not only diluted, but also present in various crystal structures that offer differing connectivity of the metal centres, thereby offering the possibility of developing structure-property relationships to optimise electrocatalytic behaviour. While a number of recent reviews have examined various aspects of the development and implementation of new oxides of ruthenium and iridates specifically for acid-resilient electrocatalysts (2–4, 7, 56–60), it is the purpose of this two-part article to survey the various crystalline structures recently discovered for iridium and ruthenium oxides, to consider their synthesis and to summarise some of the mechanistic findings made, with emphasis of the degradation pathways of the new oxide electrocatalysts that have emerged. This will include some of our own work on the use of solution-based synthesis methods for formation of mixed-metal oxide materials.

2. Survey of Ruthenium and Iridium Oxide Structures for Oxygen Evolution Reaction Catalysis

The crystal chemistry of ruthenium and iridium oxides is associated with a range of possible oxidation states of the pgm, each of which may have various coordination preferences, in turn leading to distinctive structural chemistry (61, 62). For ruthenium, in Group 7, oxidation states in oxides can range from as low as +2, reported in the phase $SrFe_{0.5}Ru_{0.5}O_2$, formed by topochemical reduction of perovskite $SrFe_{0.5}Ru_{0.5}O_3$ using CaH_2 (63), up to +8 as seen in RuO_4, although most commonly the oxide chemistry is dominated by the +4 and +5 oxidation states for ruthenium. In the case of iridium in Group 8, a smaller range of oxidation states is seen: from +3 to +6 (although it may be noted that molecular IrO_4, containing the +8 oxidation state was isolated in noble gas matrices at extremely low temperatures (64), and even the +9 oxidation state detected in the species $[IrO_4]^+$ in the gas phase (65)). As was mentioned above, the rutile structure-type is found for the metal dioxides of both ruthenium and iridium, and the +4 oxidation state appears most stable for a binary oxide of each of the two elements. Other binary oxides of ruthenium and iridium are less well-characterised, with evidence for Ru_2O_3 and Ir_2O_3 as distinct crystalline phases not compelling.

Instead, a variety of structures of ternary and higher oxides of ruthenium and iridium are found,

where electropositive partner cations, such as alkali, alkaline earth or rare earth metals, promote increased orbital overlap between oxygen and the electronegative pgms by destabilisation of the O-p states, which may provide a means of stabilising higher oxidation states of the pgm, as discussed by Kurzman *et al*. (66). In these materials, a variety of local structural arrangements may also be possible, such as the connectivity of pgm coordination polyhedra, which in turn may provide novel electrocatalytic properties. As well as diluting the amount of pgm, the substitutional chemistry possible in mixed-metal oxides to form solid-solutions or an isomorphous series of materials, provides a means of tuning structural chemistry, such as local atomic environment (bond distances and local symmetry), and average pgm oxidation state (which will adjust the number of d electrons for conductivity, and the metal-oxide bond strength). **Table I** summarises and compares the various crystal structure types that we will consider, and these will be described in more detail in the following paragraphs, with examples of chemical compositions provided.

Oxide materials with the $A_2B_2O_6O'$ pyrochlore structure stand out as being of use for many heterogeneous catalysis applications, as well as being of interest for their electronic and magnetic properties (67). The pyrochlore structure may be viewed as an oxygen deficient fluorite $A_2B_2O_{8-1}$ where half the cations (B) have coordination number 6 and the remainder (A) maintain their coordination number of 8. Depending on the positions of the oxide ions, the B sites may have regular octahedral geometry accompanied by irregular 6+2 coordination for the A site, or rather the B site may be distorted octahedral and the A-site a cubic 8-coordinate site. For the former case, the structure may be viewed as constructed from corner-shared BO_6 octahedra that create a network that incorporates the A site cations along with additional oxide ions, **Figure 2**.

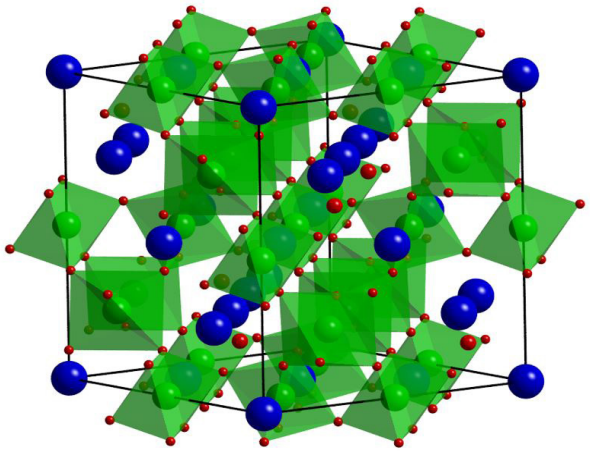

Fig. 2. The cubic unit cell of the $A_2B_2O_7$ pyrochlore structure showing the corner-shared connectivity of the B-site octahedra (green, ruthenium or iridium in ruthenates and iridates), with A-site cations as blue spheres and additional oxide ions as the larger red spheres

Table I Crystal Structures of Ruthenate and Iridates Studied as Oxygen Evolution Reaction Electrocatalysts

Structure type	Ideal chemical composition	A-site coordination environment	B-site coordination environment (ruthenium or iridium)	Ruthenium/ iridium oxidation state	Examples
Rutile	BO_2	–	Corner- and edge-shared octahedra	+4	RuO_2 IrO_2
Pyrochlore	$A_2B_2O_6O'$	8-coordinate	Corner-shared octahedra	+4 or +5	$Bi_2Ir_2O_7$ $Ln_2Ir_2O_7$ (Ln = La, Nd, Pr) $(Na,Ca)_2Ir_2O_6{\cdot}H_2O$
Perovskite	ABO_3	12-coordinate	Corner-shared octahedra	+3, +4 or +5	$SrIr_{0.8}Zn_{0.2}O_3$ $LaRuO_3$
Ruddlesden-Popper	$A_{n+1}B_nO_{3n+1}$	12-coordinate or 9-coordinate	Corner-shared octahedra	+4 or +5	Sr_2IrO_4 $Sr_3Ir_2O_7$
Hexagonal perovskite	ABO_3	Distorted 12-coordinate	Face-shared and corner-shared octahedra	+4	6H-$SrIrO_3$ 9R-$BaIrO_3$
α-Li_2IrO_3	A_2BO_3	6-coordinate, octahedral	Edge-shared octahedra	+4	Li_2IrO_3
Hollandite	A_xBO_2	Distorted 8-coordinate	Edge-shared and corner-shared octahedra	+4 or +5	$K_{0.25}IrO_2$

There are a variety of possible combinations of A and B metals in the pyrochlore structure, and oxygen non-stoichiometry is possible by partial occupation of the O' site, or replacement of oxide by hydroxide or water leading to inherently defective materials with redox properties for the B-site metal and pathways for oxide-ion migration in the solid-state. Partnering iridium on the B-site with a range of A-site metals offers the possibility of tuning crystal chemistry, electronic structure and, potentially, surface chemistry to optimise electrocatalysis properties (68). We have previously described the electrocatalytic activity of the pyrochlore $Bi_2Ir_2O_7$, prepared *via* a facile hydrothermal route (69), and the mixed ruthenate-iridate phases $(Na_{0.33}Ce_{0.67})_2(Ir_{1-x}Ru_x)_2O_7$ (70). This led to the discovery of phases $(Na,Ca)_{2-x}(Ir_{2-y}M_y)O_6{\cdot}nH_2O$ (M = antimony, zirconium, ruthenium, rhodium) that offer favourable OER activities when fabricated into MEAs, with certain compositions minimising the unfavourable carbon corrosion reaction (71, 72).

Sun *et al.* compared the OER activity of the pyrochlores $Bi_2Ir_2O_7$ and $Pb_2Ir_2O_{6.5}$ with IrO_2 and proposed a correlation of OER activity with the local atomic distortion of iridium environment (73). Lebedev *et al.* prepared $Y_2Ir_2O_7$, $Bi_2Ir_2O_7$ and $Pb_2Ir_2O_7$, including mixed A-site variants of these end members, and produced electrocatalysts with OER activities approaching that of IrO_2 nanoparticles in acid conditions (74). Shang *et al.* studied $R_2Ir_2O_7$ (R = holmium, terbium, gadolinium, neodymium and praseodymium) and proposed that $Pr_2Ir_2O_7$ was most active due to enhanced covalency in Ir–O bonds and a higher conductivity (75). Abbot *et al.* compared the iridate pyrochlores with ruthenate analogues with A-site neodymium, gadolinium or ytterbium and found all to be more stable than IrO_2, with the ruthenates and $Yb_2Ir_2O_7$ being more active (76). The pyrochlores are also active towards OER in alkali conditions: Parrondo *et al.* studied $A_2B_2O_{7-y}$ (A = lead or bismuth, and B = ruthenium, iridium or osmium) for OER and correlated activity with composition (77).

Various B-site ruthenate pyrochlores have been prepared as OER electrocatalysts, including with the trivalent A-site cations yttrium, neodymium, gadolinium, bismuth (78–80), implying an oxidation of +4 for ruthenium. A-site substitution has also been investigated for these materials with materials $Y_{2-x}M_xRu_2O_{7-\delta}$ formed for M = zinc (78), M = copper, cobalt, nickel, iron (81), M = barium (82), M = strontium (83), and M = magnesium (84). With these divalent substituents the charge may be compensated by oxide-ion deficiencies, as indicated by the chemical formula, but there is also the possibility of partial oxidation of ruthenium to the +5 oxidation state, or higher, as seen in the phase $Ca_{1.5}Ru_2O_7$ (85). Mixed ruthenium-iridium pyrochlores have also been studied, and a synergistic effect of combining the two cations was investigated in the materials $A_2B_2O_7$ with A = neodymium, gadolinium or ytterbium and B = $Ir_{1-x}Ru_x$ with x = 0.2, 0.4, 0.6, 0.8 (86).

The ABO_3 perovskite structure is common in solid-state chemistry, and consists of a corner-shared network of BO_6 octahedra in which the 12-coordinate A-site cations are found, **Figure 3(a)** (87). The versatility of the perovskite structure arises from the degree of tilting of the

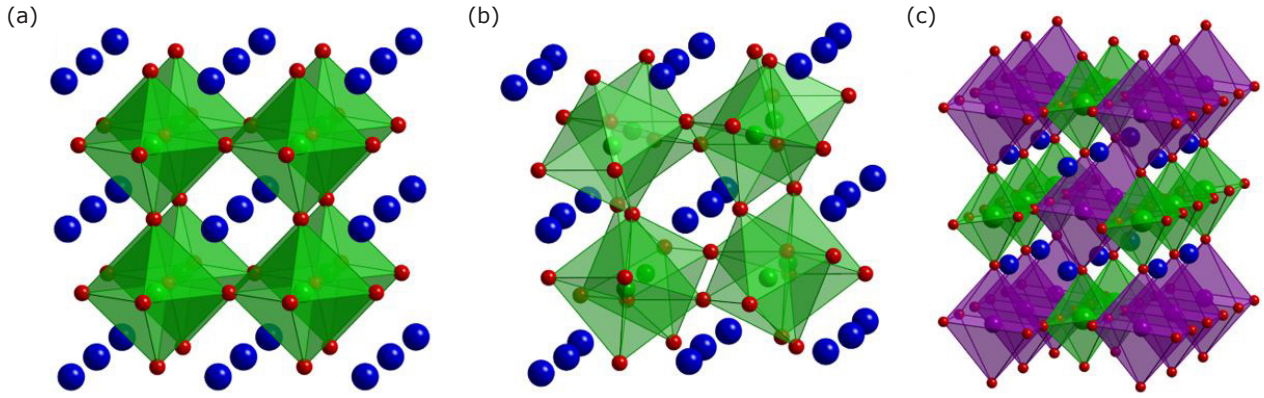

Fig. 3. Polyhedral views of ABO_3 perovskite structures: (a) the cubic parent structure; (b) orthorhombic distorted perovskite from octahedral tilting; (c) an ordered double perovskite structure $A_2BB'O_6$. The green octahedra would be occupied by ruthenium or iridium in ruthenates and iridates and the A-site cations are shown as blue spheres. The red spheres are oxide ions and the purple octahedra in (b) contain the second B-site cation (see text)

octahedra to give a range of possible B-O-B angles, lowering the coordination of the A-site to allow accommodation of smaller cations, **Figure 3(b)**. For ruthenate and iridate perovskites, with their preference for octahedral coordination, ruthenium and iridium are expected to be found on the B-site, although in fact the perovskite phases that have been prepared for electrocatalysis are more complex solid solutions or substitutional series. $SrIrO_3$ as a perovskite phase was prepared as an epitaxial layer on $SrTiO_3$ as substrate using pulsed laser deposition by Seitz *et al*. (88). Pseudocubic $SrIrO_3$ thin films were also grown on (La,Sr)(Al,Ta)O_3 substrates by molecular-beam epitaxy (89). Orthorhombic $SrIr_{0.8}Zn_{0.2}O_3$ (90) and the cubic phase $SrTi_{0.67}Ir_{0.33}O_3$ (91) are examples of bulk materials with the classical perovskite structure, and the former contains mixed-valent iridium, formally in the +4.5 oxidation state. The $SrTiO_3$-$SrIrO_3$ solid solution has been produced in the form of nanotubes (92). The orthorhombic ruthenate perovskites $LaRuO_3$ (93), $SrRuO_3$, $Sr_{0.95}Na_{0.05}RuO_3$ and $S_{0.90}Na_{0.10}RuO_3$ (94) have been studied and the oxidation state of ruthenium depends on the choice of A-site cation(s).

With certain combinations of metal cations, double perovskites can be produced where the B-site cations form an ordered superstructure, **Figure 3(c)**. Examples of iridates and ruthenates include the sets of materials Ba_2MIrO_6 M = yttrium, lanthanum, cerium, praseodymium, neodymium and terbium (95), A_2BIrO_6 (A = praseodymium, neodymium or yttrium; B = barium or strontium) (96), Sr_2MIrO_6 (M= iron, cobalt) (97), La_2LiMO_6 (M = iridium or ruthenium) (98), A_2BIrO_6, (A = barium and strontium; B =lanthanides, yttrium and tin) (99), and Sr_2MIrO_6 (M = nickel, cobalt, scandium and iron) (100). Less commonly, the A-site cations may be ordered, and the phase $CaCu_3Ir_4O_{12}$ provides an example, studied for OER electrocatalysis under alkaline conditions (101). The analogous ruthenate, $CaCu_3Ru_4O_{12}$, on the other hand, has shown high activity and stability for OER under acid conditions (102).

Related to the perovskite structure are the Ruddlesden-Popper phases, **Figure 4** (103). These have general chemical formula $A_{n+1}B_nX_{3n+1}$ where A and B are appropriate cations (B will be iridium or ruthenium in this discussion) and X an anion, oxide in this case. The Ruddlesden–Popper structure may be viewed as a layered variant of the perovskite structure, where sheets of corner-shared B-centred octahedra are interleaved with rock-salt (NaCl type) layers of A-centred octahedra and so may

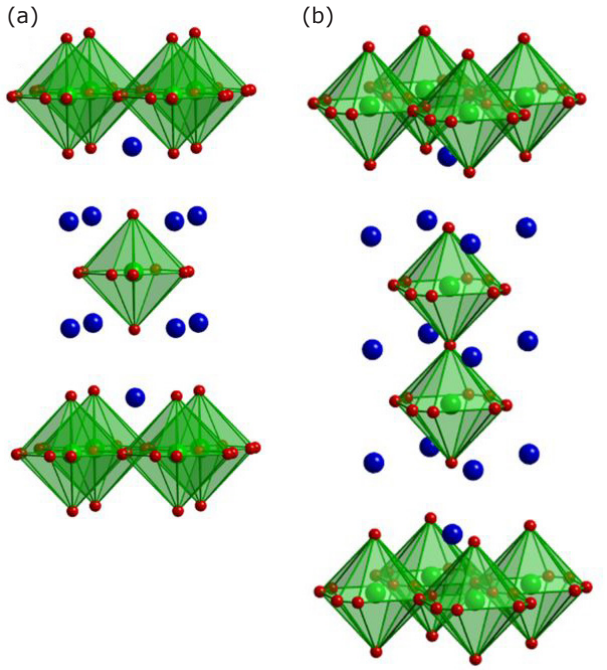

Fig. 4. Ruddlesden–Popper structures $n(ABX_3)_n{\cdot}AX$ for: (a) n = 1, as found for Sr_2IrO_4; and (b) n = 2, as found for $Sr_3Ir_2O_7$. The green octahedra would be occupied by ruthenium or iridium in ruthenates and iridates and the A-site cations are shown as blue spheres

be written $(ABX_3)_n{\cdot}AX$. The n = ∞ composition corresponds to the conventional perovskite structure. For n = 1, the iridates Sr_2IrO_4 (95, 104) Ca_2IrO_4 (105) and $Sr_2Fe_{0.5}Ir_{0.5}O_4$ (97) have been reported, with the first two containing Ir^{4+} and the last, Ir^{5+}. Ion-exchange of Sr_2IrO_4 using aqueous perchloric acid leads to the protonated n = 1 Ruddlesden-Popper phase $H_{3.6}IrO_4{\cdot}3.7H_2O$ (106). The n = 2 Ruddlesden-Popper $Sr_3Ir_2O_7$ has also been studied for its OER activity (107).

Another set of so-called perovskite phases have the ABO_3 chemical composition but different connectivity of the octahedral building units. An example is $SrIrO_3$, whose structure is an example of a hexagonal perovskite, **Figure 5(a)**, in this case of the 6H type, where alternating face-sharing IrO_6 octahedral dimers corner-share with isolated IrO_6 octahedra. The structure is actually monoclinic, being a distorted version of the 6H-$BaTiO_3$ structure, where iridium–iridium metal-metal bonding is present in the face-shared IrO_6 octahedra. It is only by B-site substitution that the classical perovskite structure is produced for $SrIrO_3$ under ambient pressure, such as with Ti^{4+}, or Zn^{2+}, as mentioned above (108). 6H-$SrIrO_3$ has been synthesised as a polycrystalline powder and studied by a number of authors (89, 104,

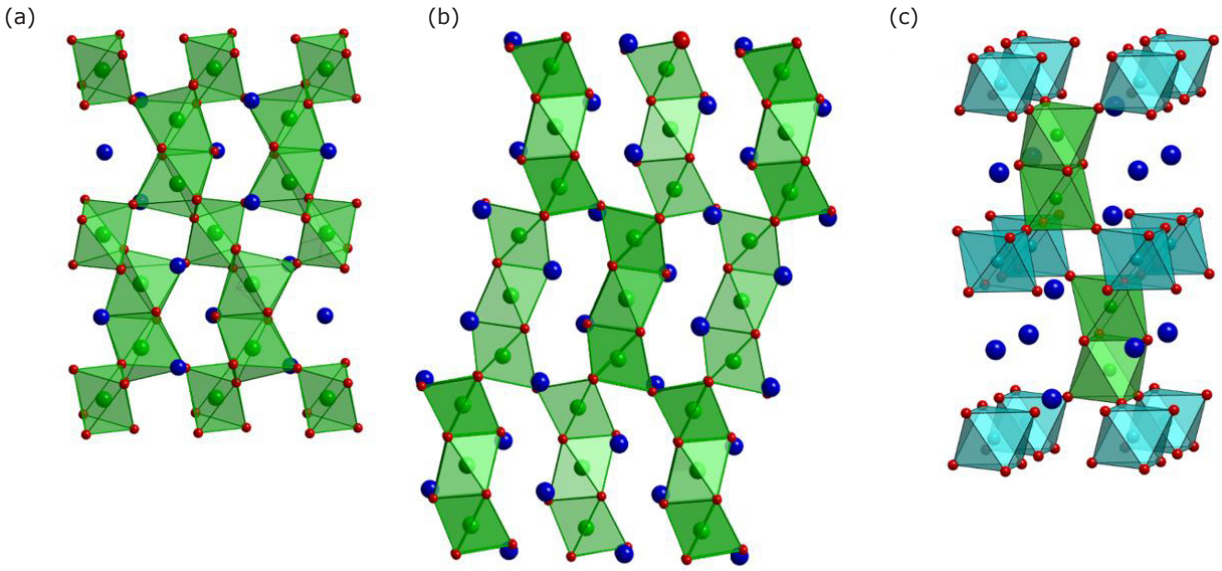

Fig. 5. Examples of iridates with hexagonal perovskite structures: (a) 6H-$SrTiO_3$ (drawn using the idealised 6H-$BaTiO_3$ structure); (b) 9R-$BaIrO_3$; (c) the triple perovskite $Ba_3IrTi_2O_9$. In all cases the green polyhedra represent octahedrally coordinated iridium with red oxide, and the blue spheres are the alkali-metal cations. The blue polyhedra in (c) are titanium-centred octahedra

109–111). Recently, $SrIrO_3$ was modified with Ruddlesden-Popper Sr_2IrO_4 to give a composite two-phase sample (112).

$BaIrO_3$ has likewise been studied, and this phase exists in the 9R polymorph when prepared at ambient pressure, **Figure 5(b)**, also of monoclinic crystal system, but with trimers of face-shared octahedra (89). Amorphous IrO_x on 9R-$BaIrO_3$ was found to be a particularly active electrocatalyst (113). The triple perovskites $Ba_3M'M''_2O_9$ (M' = titanium, indium or zinc; M'' = IrIr, IrTi, IrRu or RuRu) have structures consisting of face-shared M''_2O_9 dimers and isolated $M'O_6$ octahedra, **Figure 5(c)** (114). $Ba_4MIr_3O_{12}$ with M = praseodymium, bismuth, niobium adopt 12L-perovskite structures with isolated trinuclear Ir_3O_{12} units with MO_6 octahedra alternately linked in a corner-sharing fashion, thus generating the 12-layer structure (115). $La_{3.5}Ru_4O_{13}$ and La_2RuO_5 are further examples of materials with perovskite-derived structures that have been prepared for investigation as OER electrocatalysts (93).

Various other ruthenate and iridate complex oxides have been studied, although none as systematically as the rutiles, pyrochlores and perovskites described so far. This includes materials with fluorite-related structures, Ln_3IrO_7 with Ln = neodymium, europium (54) or praseodymium (95), which contain Ir^{5+}. More open structures have also been considered, including those with tunnel-like structures, such as potassium iridate hollandites (116, 117), **Figure 6(a)**. In the case of layered α-Li_2IrO_3, **Figure 6(b)**, ion-exchange with potassium in alkali conditions yields a birnessite-type structure (118). The spinel $NiCo_{2-x}O_4$ has been substituted with iridium (119). Some other iridate compositions with crystalline structures, such as Sr_4IrO_6 with isolated iridium-centred octahedra (104), have also been studied. Finally, composite materials have been considered, where a two-phase mixture of oxides is purposely produced, examples being iridium-tungsten oxide (120), and a mixed-phase $BaIrO_{2.937}/La_3IrO_7$ material consisting of hexagonal perovskite and fluorite-structured materials (121).

3. Synthesis Methods for Oxides of Ruthenium and Iridium

As with many ternary and higher mixed-metal oxides, the simplest approach to synthesis is from the individual, binary oxides, *via* a solid-state reaction. This requires intimate grinding or milling of the solid precursors to ensure homogeneity, heating to high temperature, often in excess of 1000°C, followed by cycles of regrinding and reheating until phase-pure crystalline material is produced. Examples of materials produced by such methods include the iridate perovskites La_2LiIrO_6 (98), Ba_2MIrO_6 (M = yttrium, lanthanum, cerium, praseodymium, neodymium and terbium) (95), A_2BIrO_6 (A = praseodymium, neodymium or

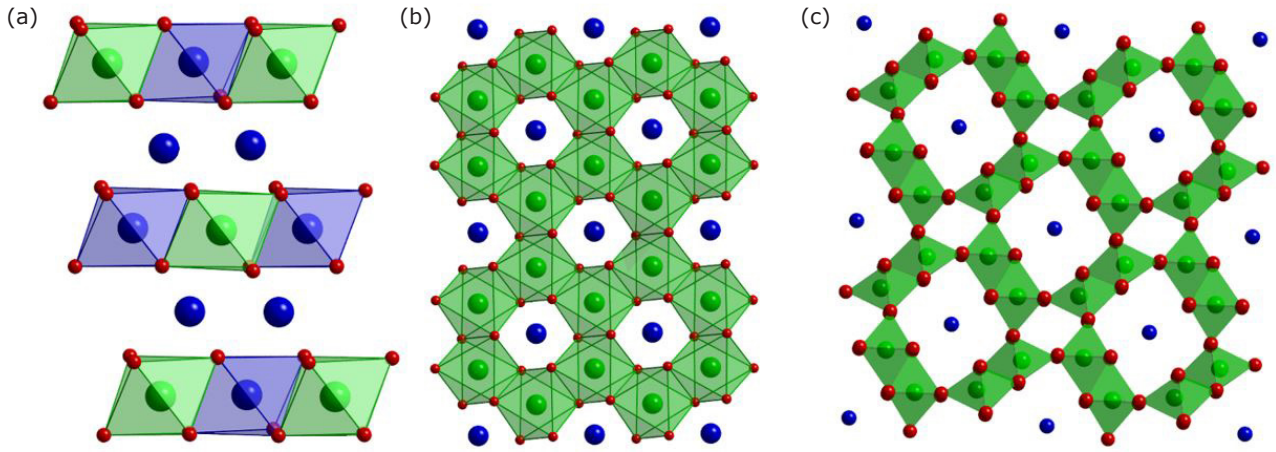

Fig. 6. Iridates with open structures: (a) view of layered α-Li_2IrO_3 parallel to layers with blue octahedra containing lithium, green octahedra containing iridium and blue spheres representing lithium interlayer; (b) view of layered α-Li_2IrO_3 perpendicular to layers, showing iridium oxide honeycomb structure; and (c) the hollandite tunnel structure with blue spheres representing the occluded ions, such as potassium

yttrium; B = barium or strontium) (96), $Ba_3MM_2O_9$ (M= titanium, indium or zinc; M_2 = IrIr, IrTi, IrRu or RuRu) (114), and the hexagonal perovskites $AIrO_3$ (A = strontium or barium) (89) and 12L-$Ba_4MIr_3O_{12}$ (M = praseodymium, bismuth, niobium) (115). Such reactions may be facilitated by using carbonate precursors, where the loss of gaseous CO_2 provides an additional entropic driving force for the reaction. Disadvantages of such a synthesis approach are that volatility of any of the component binary oxides may result in loss of material so that metal ratios are difficult to control, and that crystallite growth is unpredictable and difficult to control so that typically large crystallites with low surface area are produced. Furthermore, only the most thermodynamically stable phases are accessed under such conditions limiting the range of possible compositions that might be available. Mechanical activation may be used to ensure greater homogeneity of precursors and lower the temperature of synthesis, such as in the case of $SrIrO_3$ (110). In other cases, high pressure must be employed to drive the reaction and an example is provided by the case of $Sr_3Ir_2O_7$ (107).

Low temperature routes to solid state materials have been developed to allow control of homogeneity and formation of materials with small crystallite size and high surface area and examples are the cases of coprecipitation and sol-gel methods, where a disordered precursor is formed from a solution and then subsequently heat treated under moderate temperature to yield the desired crystalline phase. This has been less studied than solid-state synthesis for iridates, but the cases of 6H-$SrIrO_3$ (109), Sr_2MIrO_6 (M = nickel, cobalt, scandium and iron) (100) and $SrTi_{0.67}Ir_{0.33}O_3$ (91) illustrate this approach. Hydrothermal synthesis employs solution chemistry in combination with heat treatment in a sealed vessel to generate a moderate pressure and under these conditions the formation of many multinary oxides has proved possible including a number of ruthenium and iridium oxides (122). The method has been particularly useful for the preparation of pyrochlore phases, as we have shown in our own work, leading to the discovery of a variety of new compositions for both iridium and ruthenium materials, and mixed ruthenate-iridates (70, 71, 85, 123, 124), as well as being applied for the convenient preparation of others that would usually be formed at high temperature (69, 73, 125). The solids are typically produced as fine powders with crystallites of only a few tens of nanometres in dimension meaning that they can be easily dispersed with a polymer binder, for example, and employed in an electrochemical device. In some cases molten salts can be used for the formation of mixed oxide materials and the Adams fusion method has been used for the crystallisation of some iridium oxides using molten $NaNO_3$ as a reaction medium. Here, temperatures of around 500°C are used and this has allowed the formation of materials such as pyrochlores $(B,Pb,Y)_2Ir_2O_{6-x}$ (74). A spray-freeze, freeze-drying technique has also been applied to prepare mixed ruthenium-iridium pyrochlores $A_2(Ru,Ir)_2O_7$ with A = ytterbium, gadolinium or neodymium with particle size in the submicron regime (86). While not every synthesis approach may be applicable to every composition it is apparent that there exists a wide choice of preparative chemistry suited for

the formation of oxides of iridium and ruthenium. For the formation of layers and thin films, more complex experimental design is required. Seitz *et al.* produced films of $SrIrO_3$ by epitaxial growth on $SrTiO_3$ using pulsed laser deposition from a $SrIrO_3$ polycrystalline target (88), while pseudocubic $SrIrO_3$ thin films were grown on $(La,Sr)(Al,Ta)O_3$ substrates by molecular-beam epitaxy (89). The majority of iridate and ruthenate materials have been formed, however, as polycrystalline powders and layer deposition has not yet been reported for many of the complex compositions recently studied.

Part II (126) will cover mechanistic details and acid stability of pgm oxides and the conclusions and outlook.

Acknowledgements

We thank our colleagues at Johnson Matthey, particularly the group of Jonathan Sharman, for their continued collaboration in work in this field. Jasmine Clayton thanks Johnson Matthey for part funding of a PhD studentship with the EPSRC Doctoral Training Partnership award EP/R513374/1. Richard Walton thanks the Royal Society for provision of an Industry Fellowship with Johnson Matthey during which some of ideas in this article were developed.

References

1. J. Song, C. Wei, Z.-F. Huang, C. Liu, L. Zeng, X. Wang and Z. J. Xu, *Chem. Soc. Rev.*, 2020, **49**, (7), 2196
2. Z. Lei, T. Wang, B. Zhao, W. Cai, Y. Liu, S. Jiao, Q. Li, R. Cao and M. Liu, *Adv. Energy Mater.*, 2020, **10**, (23), 2000478
3. Y. Zhang, X. Zhu, G. Zhang, P. Shi and A.-L. Wang, *J. Mater. Chem. A*, 2021, **9**, (10), 5890
4. Z. Pu, T. Liu, G. Zhang, H. Ranganathan, Z. Chen and S. Sun, *ChemSusChem*, 2021, **14**, (21), 4636
5. M. Carmo, D. L. Fritz, J. Mergel and D. Stolten, *Int. J. Hydrogen Energy*, 2013, **38**, (12), 4901
6. M. B. Karimi, F. Mohammadi and K. Hooshyari, *Int. J. Hydrogen Energy*, 2019, **44**, (54), 28919
7. T. Reier, H. N. Nong, D. Teschner, R. Schlögl and P. Strasser, *Adv. Energy Mater.*, 2016, **7**, (1), 1601275
8. W. Gu, P. T. Yu, R. N. Carter, R. Makharia and H. A. Gasteiger, 'Modeling of Membrane-Electrode-Assembly Degradation in Proton-Exchange-Membrane Fuel Cells – Local H_2 Starvation and Start–Stop Induced Carbon-Support Corrosion', in "Modeling and Diagnostics of Polymer Electrolyte Fuel Cells", eds. U. Pasaogullari and C.-Y. Wang, Modern Aspects of Electrochemistry Series, No. 49, Ch. 2, Springer Science and Business Media LLC, New York, NY, 2009, pp 45–87
9. R. T. Atanasoski, L. L. Atanasoska and D. A. Cullen, 'Efficient Oxygen Evolution Reaction Catalysts for Cell Reversal and Start/Stop Tolerance', in "Electrocatalysis in Fuel Cells: A Non- and Low-Platinum Approach", ed. M. Shao, Lecture Notes in Energy Book Series, Vol. 9, Springer Verlag, London, UK, 2013, pp 637–664
10. T. C. Crowtz, D. A. Stevens, R. J. Sanderson, J. E. Harlow, G. D. Vernstrom, L. L. Atanasoska, G. M. Haugen, R. T. Atanasoski and J. R. Dahn, *J. Electrochem. Soc.*, 2014, **161**, (10), F961
11. J. Park, M. Park, G. Nam, M. G. Kim and J. Cho, *Nano Lett.*, 2017, **17**, (6), 3974
12. N.-T. Suen, S.-F. Hung, Q. Quan, N. Zhang, Y.-J. Xu and H. M. Chen, *Chem. Soc. Rev.*, 2017, **46**, (2), 337
13. X.-K. Gu, J. C. A. Camayang, S. Samira and E. Nikolla, *J. Catal.*, 2020, **388**, 130
14. S. Back, K. Tran and Z. W. Ulissi, *ACS Appl. Mater. Interfaces*, 2020, **12**, (34), 38256
15. L. Wang, V. A. Saveleva, S. Zafeiratos, E. R. Savinova, P. Lettenmeier, P. Gazdzicki, A. S. Gago and K. A. Friedrich, *Nano Energy*, 2017, **34**, 385
16. R. Kötz and S. Stucki, *Electrochim. Acta*, 1986, **31**, (10), 1311
17. L.-E. Owe, M. Tsypkin, K. S. Wallwork, R. G. Haverkamp and S. Sunde, *Electrochim. Acta*, 2012, **70**, 158
18. O. Kasian, S. Geiger, P. Stock, G. Polymeros, B. Breitbach, A. Savan, A. Ludwig, S. Cherevko and K. J. J. Mayrhofer, *J. Electrochem. Soc.*, 2016, **163**, (11), F3099
19. S. Cherevko, S. Geiger, O. Kasian, N. Kulyk, J.-P. Grote, A. Savan, B. R. Shrestha, S. Merzlikin, B. Breitbach, A. Ludwig and K. J. J. Mayrhofer, *Catal. Today*, 2016, **262**, 170
20. A. H. Reksten, H. Thuv, F. Seland and S. Sunde, *J. Electroanal. Chem.*, 2018, **819**, 547
21. D. F. Abbott, D. Lebedev, K. Waltar, M. Povia, M. Nachtegaal, E. Fabbri, C. Copéret and T. J. Schmidt, *Chem. Mater.*, 2016, **28**, (18), 6591
22. G. C. da Silva, N. Perini and E. A. Ticianelli, *Appl. Catal. B: Environ.*, 2017, **218**, 287
23. Y. Lee, J. Suntivich, K. J. May, E. E. Perry and Y. Shao-Horn, *J. Phys. Chem. Lett.*, 2012, **3**, (3), 399

24. J. Ahmed and Y. Mao, *Electrochim. Acta*, 2016, **212**, 686
25. P. Steegstra, M. Busch, I. Panas and E. Ahlberg, *J. Phys. Chem. C*, 2013, **117**, (40), 20975
26. S. Cherevko, S. Geiger, O. Kasian, A. Mingers and K. J. J. Mayrhofer, *J. Electroanal. Chem.*, 2016, **774**, 102
27. E. Willinger, C. Massué, R. Schlögl and M. G. Willinger, *J. Am. Chem. Soc.*, 2017, **139**, (34), 12093
28. P. E. Pearce, C. Yang, A. Iadecola, J. Rodriguez-Carvajal, G. Rousse, R. Dedryvère, A. M. Abakumov, D. Giaume, M. Deschamps, J.-M. Tarascon and A. Grimaud, *Chem. Mater.*, 2019, **31**, (15), 5845
29. J. Gao, C.-Q. Xu, S.-F. Hung, W. Liu, W. Cai, Z. Zeng, C. Jia, H. M. Chen, H. Xiao, J. Li, Y. Huang and B. Liu, *J. Am. Chem. Soc.*, 2019, **141**, (7), 3014
30. A. De Battisti, A. Barbieri, A. Giatti, G. Battaglin, S. Daolio and A. B. Boscoletto, *J. Mater. Chem.*, 1991, **1**, (2), 191
31. E. Oakton, D. Lebedev, M. Povia, D. F. Abbott, E. Fabbri, A. Fedorov, M. Nachtegaal, C. Copéret and T. J. Schmidt, *ACS Catal.*, 2017, **7**, (4), 2346
32. S. Ferro, D. Rosestolato, C. A. Martínez-Huitle and A. De Battisti, *Electrochim. Acta*, 2014, **146**, 257
33. G. Li, H. Yu, D. Yang, J. Chi, X. Wang, S. Sun, Z. Shao and B. Yi, *J. Power Sources*, 2016, **325**, 15
34. M. E. C. Pascuzzi, J. P. Hofmann and E. J. M. Hensen, *Electrochim. Acta*, 2021, **366**, 137448
35. H. Sun and W. Jung, *J. Mater. Chem. A*, 2021, **9**, (28), 15506
36. K. Macounová, M. Makarova, J. Jirkovský, J. Franc and P. Krtil, *Electrochim. Acta*, 2008, **53**, (21), 6126
37. M. V. Makarova, J. Jirkovský, M. Klementová, I. Jirka, K. Macounová and P. Krtil, *Electrochim. Acta*, 2008, **53**, (5), 2656
38. V. Petrykin, Z. Bastl, J. Franc, K. Macounova, M. Makarova, S. Mukerjee, N. Ramaswamy, I. Spirovova and P. Krtil, *J. Phys. Chem. C*, 2009, **113**, (52), 21657
39. V. Petrykin, K. Macounová, M. Okube, S. Mukerjee and P. Krtil, *Catal. Today*, 2013, **202**, 63
40. L. K. McLeod, G. H. Spikes, R. J. Kashtiban, M. Walker, A. V. Chadwick, J. D. B. Sharman and R. I. Walton, *Dalt. Trans.*, 2020, **49**, (8), 2661
41. D. L. Burnett, E. Petrucco, K. M. Rigg, C. M. Zalitis, J. G. Lok, R. J. Kashtiban, M. R. Lees, J. D. B. Sharman and R. I. Walton, *Chem. Mater.*, 2020, **32**, (14), 6150
42. Y.-Y. Feng, S. Si, G. Deng, Z.-X. Xu, Z. Pu, H.-S. Hu and C.-B. Wang, *J. Alloys Compd.*, 2022, **892**, 162113
43. Y. Lin, Z. Tian, L. Zhang, J. Ma, Z. Jiang, B. J. Deibert, R. Ge and L. Chen, *Nat. Commun.*, 2019, **10**, 162
44. N. B. Halck, V. Petrykin, P. Krtil and J. Rossmeisl, *Phys. Chem. Chem. Phys.*, 2014, **16**, (27), 13682
45. Y. Wen, P. Chen, L. Wang, S. Li, Z. Wang, J. Abed, X. Mao, Y. Min, C. T. Dinh, P. De Luna, R. Huang, L. Zhang, L. Wang, L. Wang, R. J. Nielsen, H. Li, T. Zhuang, C. Ke, O. Voznyy, Y. Hu, Y. Li, W. A. Goddard, B. Zhang, H. Peng and E. H. Sargent, *J. Am. Chem. Soc.*, 2021, **143**, (17), 6482
46. T. Audichon, S. Morisset, T. W. Napporn, K. B. Kokoh, C. Comminges and C. Morais, *ChemElectroChem*, 2015, **2**, (8), 1128
47. D. Escalera-López, S. Czioska, J. Geppert, A. Boubnov, P. Röse, E. Saraçi, U. Krewer, J.-D. Grunwaldt and S. Cherevko, *ACS Catal.*, 2021, **11**, (15), 9300
48. N. Danilovic, R. Subbaraman, K. C. Chang, S. H. Chang, Y. Kang, J. Snyder, A. P. Paulikas, D. Strmcnik, Y. T. Kim, D. Myers, V. R. Stamenkovic and N. M. Markovic, *Angew. Chem. Int. Ed.*, 2014, **53**, (51), 14016
49. J. Shan, C. Guo, Y. Zhu, S. Chen, L. Song, M. Jaroniec, Y. Zheng and S.-Z. Qiao, *Chem*, 2019, **5**, (2), 445
50. H. Xu, S. Ci, Y. Ding, G. Wang and Z. Wen, *J. Mater. Chem. A*, 2019, **7**, (14), 8006
51. M. Huynh, D. K. Bediako and D. G. Nocera, *J. Am. Chem. Soc.*, 2014, **136**, (16), 6002
52. M. Huynh, C. Shi, S. J. L. Billinge and D. G. Nocera, *J. Am. Chem. Soc.*, 2015, **137**, (47), 14887
53. J. B. Goodenough, R. Manoharan and M. Paranthaman, *J. Am. Chem. Soc.*, 1990, **112**, (6), 2076
54. M. V. ten Kortenaar, J. F. Vente, D. J. W. Ijdo, S. Müller and R. Kötz, *J. Power Sources*, 1995, **56**, (1), 51
55. M. Fan, X. Liang, H. Chen and X. Zou, *Dalt. Trans.*, 2020, **49**, (44), 15568
56. R. Zhang, P. E. Pearce, Y. Duan, N. Dubouis, T. Marchandier and A. Grimaud, *Chem. Mater.*, 2019, **31**, (20), 8248
57. Z. Chen, X. Duan, W. Wei, S. Wang and B.-J. Ni, *Nano Energy*, 2020, **78**, 105270
58. L. An, C. Wei, M. Lu, H. Liu, Y. Chen, G. G. Scherer, A. C. Fisher, P. Xi, Z. J. Xu and C.-H. Yan, *Adv. Mater.*, 2021, **33**, (20), 2006328
59. L. Li, P. Wang, Q. Shao and X. Huang, *Adv. Mater.*, 2021, **33**, (50), 2004243

60. Y. Liu, X. Liang, H. Chen, R. Gao, L. Shi, L. Yang and X. Zou, *Chinese J. Catal.*, 2021, **42**, (7), 1054
61. H. Müller-Buschbaum, *Z. Anorg. Allg. Chem.*, 2005, **631**, (6–7), 1005
62. H. Müller-Buschbaum, *Z. Anorg. Allg. Chem.*, 2006, **632**, (10–11), 1625
63. F. Denis Romero, S. J. Burr, J. E. McGrady, D. Gianolio, G. Cibin and M. A. Hayward, *J. Am. Chem. Soc.*, 2013, **135**, (5), 1838
64. Y. Gong, M. Zhou, M. Kaupp and S. Riedel, *Angew. Chem. Int. Ed.*, 2009, **48**, (42), 7879
65. G. Wang, M. Zhou, J. T. Goettel, G. J. Schrobilgen, J. Su, J. Li, T. Schlöder and S. Riedel, *Nature*, 2014, **514**, (7523), 475
66. J. A. Kurzman, L. M. Misch and R. Seshadri, *Dalton Trans.*, 2013, **42**, (41), 14653
67. M. A. Subramanian, G. Aravamudan and G. V. Subba Rao, *Prog. Solid State Chem.*, 1983, **15**, (2), 55
68. M. Kim, J. Park, M. Kang, J. Y. Kim and S. W. Lee, *ACS Cent. Sci.*, 2020, **6**, (6), 880
69. K. Sardar, S. C. Ball, J. D. B. Sharman, D. Thompsett, J. M. Fisher, R. A. P. Smith, P. K. Biswas, M. R. Lees, R. J. Kashtiban, J. Sloan and R. I. Walton, *Chem. Mater.*, 2012, **24**, (21), 4192
70. K. Sardar, E. Petrucco, C. I. Hiley, J. D. B. Sharman, P. P. Wells, A. E. Russell, R. J. Kashtiban, J. Sloan and R. I. Walton, *Angew. Chem. Int. Ed.*, 2014, **53**, (41), 10960
71. D. L. Burnett, E. Petrucco, R. J. Kashtiban, S. F. Parker, J. D. B. Sharman and R. I. Walton, *J. Mater. Chem. A*, 2021, **9**, (44), 25114
72. D. L. Burnett, E. Petrucco, A. E. Russell, R. J. Kashtiban, J. D. B. Sharman and R. I. Walton, *Phys. Chem. Chem. Phys.*, 2020, **22**, (34), 18770
73. W. Sun, J.-Y. Liu, X.-Q. Gong, W.-Q. Zaman, L.-M. Cao and J. Yang, *Sci. Rep.*, 2016, **6**, 38429
74. D. Lebedev, M. Povia, K. Waltar, P. M. Abdala, I. E. Castelli, E. Fabbri, M. V. Blanco, A. Fedorov, C. Copéret, N. Marzari and T. J. Schmidt, *Chem. Mater.*, 2017, **29**, (12), 5182
75. C. Shang, C. Cao, D. Yu, Y. Yan, Y. Lin, H. Li, T. Zheng, X. Yan, W. Yu, S. Zhou and J. Zeng, *Adv. Mater.*, 2019, **31**, (6), 1805104
76. D. F. Abbott, R. K. Pittkowski, K. Macounová, R. Nebel, E. Marelli, E. Fabbri, I. E. Castelli, P. Krtil and T. J. Schmidt, *ACS Appl. Mater. Interfaces*, 2019, **11**, (41), 37748
77. J. Parrondo, M. George, C. Capuano, K. E. Ayers and V. Ramani, *J. Mater. Chem. A*, 2015, **3**, (20), 10819
78. Q. Feng, Q. Wang, Z. Zhang, Y. Xiong, H. Li, Y. Yao, X.-Z. Yuan, M. C. Williams, M. Gu, H. Chen, H. Li and H. Wang, *Appl. Catal. B: Environ.*, 2019, **244**, 494
79. M. A. Hubert, A. M. Patel, A. Gallo, Y. Liu, E. Valle, M. Ben-Naim, J. Sanchez, D. Sokaras, R. Sinclair, J. K. Nørskov, L. A. King, M. Bajdich and T. F. Jaramillo, *ACS Catal.*, 2020, **10**, (20), 12182
80. H. Liu, Z. Wang, M. Li, X. Zhao, X. Duan, S. Wang, G. Tan, Y. Kuang and X. Sun, *Sci. China Mater.*, 2021, **64**, (7), 1653
81. D. A. Kuznetsov, M. A. Naeem, P. V. Kumar, P. M. Abdala, A. Fedorov and C. R. Müller, *J. Am. Chem. Soc.*, 2020, **142**, (17), 7883
82. Q. Feng, J. Zou, Y. Wang, Z. Zhao, M. C. Williams, H. Li and H. Wang, *ACS Appl. Mater. Interfaces*, 2020, **12**, (4), 4520
83. N. Zhang, C. Wang, J. Chen, C. Hu, J. Ma, X. Deng, B. Qiu, L. Cai, Y. Xiong and Y. Chai, *ACS Nano*, 2021, **15**, (5), 8537
84. T.-R. Han, J.-J. Wu, Z.-X. Qu and X. Tang, *Chin. J. Inorg. Chem.*, 2021, **37**, (2), 285
85. C. I. Hiley, M. R. Lees, J. M. Fisher, D. Thompsett, S. Agrestini, R. I. Smith and R. I. Walton, *Angew. Chem. Int. Ed.*, 2014, **53**, (17), 4423
86. R. K. Pittkowski, D. F. Abbott, R. Nebel, S. Divanis, E. Fabbri, I. E. Castelli, T. J. Schmidt, J. Rossmeisl and P. Krtil, *Electrochim. Acta*, 2021, **366**, 137327
87. A. S. Bhalla, R. Guo and R. Roy, *Mater. Res. Innov.*, 2000, **4**, (1), 3
88. L. C. Seitz, C. F. Dickens, K. Nishio, Y. Hikita, J. Montoya, A. Doyle, C. Kirk, A. Vojvodic, H. Y. Hwang, J. K. Norskov and T. F. Jaramillo, *Science*, 2016, **353**, (6303), 1011
89. C. W. Song, H. Suh, J. Bak, H. Bin Bae and S.-Y. Chung, *Chem*, 2019, **5**, (12), 3243
90. J. Edgington, N. Schweitzer, S. Alayoglu and L. C. Seitz, *J. Am. Chem. Soc.*, 2021, **143**, (26), 9961
91. X. Liang, L. Shi, Y. Liu, H. Chen, R. Si, W. Yan, Q. Zhang, G.-D. Li, L. Yang and X. Zou, *Angew. Chem. Int. Ed.*, 2019, **58**, (23), 7631
92. H. Chen, L. Shi, X. Liang, L. Wang, T. Asefa and X. Zou, *Angew. Chem. Int. Ed.*, 2020, **59**, (44), 19654
93. M. Abreu-Sepulveda, P. Trinh, S. Malkhandi, S. R. Narayanan, J. Jorné, D. J. Quesnel, J. A. Postonr and A. Manivannan, *Electrochim. Acta*, 2015, **180**, 401
94. M. Retuerto, L. Pascual, F. Calle-Vallejo, P. Ferrer, D. Gianolio, A. G. Pereira, Á. García, J. Torrero, M. T. Fernández-Díaz, P. Bencok, M. A. Peña, J. L. G. Fierro and S. Rojas, *Nat. Commun.*, 2019, **10**, 2041

95. O. Diaz-Morales, S. Raaijman, R. Kortlever, P. J. Kooyman, T. Wezendonk, J. Gascon, W. T. Fu and M. T. M. Koper, *Nat. Commun.*, 2016, **7**, 12363
96. S. Geiger, O. Kasian, M. Ledendecker, E. Pizzutilo, A. M. Mingers, W. T. Fu, O. Diaz-Morales, Z. Li, T. Oellers, L. Fruchter, A. Ludwig, K. J. J. Mayrhofer, M. T. M. Koper and S. Cherevko, *Nat. Catal.*, 2018, **1**, (7), 508
97. R. Zhang, N. Dubouis, M. Ben Osman, W. Yin, M. T. Sougrati, D. A. D. Corte, D. Giaume and A. Grimaud, *Angew. Chem. Int. Ed.*, 2019, **58**, (14), 4571
98. A. Grimaud, A. Demortière, M. Saubanère, W. Dachraoui, M. Duchamp, M.-L. Doublet and J.-M. Tarascon, *Nat. Energy*, 2016, **2**, (1), 16189
99. J. G. Vos, Z. Liu, F. D. Speck, N. Perini, W. Fu, S. Cherevko and M. T. M. Koper, *ACS Catal.*, 2019, **9**, (9), 8561
100. M. Retuerto, L. Pascual, O. Piqué, P. Kayser, M. A. Salam, M. Mokhtar, J. A. Alonso, M. Peña, F. Calle-Vallejo and S. Rojas, *J. Mater. Chem. A*, 2021, **9**, (5), 2980
101. X. Ye, S. Song, L. Li, Y.-C. Chang, S. Qin, Z. Liu, Y.-C. Huang, J. Zhou, L. Zhang, C.-L. Dong, C.-W. Pao, H.-J. Lin, C.-T. Chen, Z. Hu, J.-Q. Wang and Y. Long, *Chem. Mater.*, 2021, **33**, (23), 9295
102. X. Miao, L. Zhang, L. Wu, Z. Hu, L. Shi and S. Zhou, *Nat. Commun.*, 2019, **10**, 3809
103. X. Xu, Y. Pan, Y. Zhong, R. Ran and Z. Shao, *Mater. Horiz.*, 2020, **7**, (10), 2519
104. A. L. Strickler, D. Higgins and T. F. Jaramillo, *ACS Appl. Energy Mater.*, 2019, **2**, (8), 5490
105. Y. Wu, W. Sun, Z. Zhou, W. Q. Zaman, M. Tariq, L. Cao and J. Yang, *ACS Omega*, 2018, **3**, (3), 2902
106. R. Zhang, P. E. Pearce, V. Pimenta, J. Cabana, H. Li, D. A. D. Corte, A. M. Abakumov, G. Rousse, D. Giaume, M. Deschamps and A. Grimaud, *Chem. Mater.*, 2020, **32**, (8), 3499
107. C. Zhu, H. Tian, B. Huang, G. Cai, C. Yuan, Y. Zhang, Y. Li, G. Li, H. Xu and M.-R. Li, *Chem. Eng. J.*, 2021, **423**, 130185
108. I. Qasim, B. J. Kennedy and M. Avdeev, *J. Mater. Chem. A*, 2013, **1**, (9), 3127
109. L. Yang, G. Yu, X. Ai, W. Yan, H. Duan, W. Chen, X. Li, T. Wang, C. Zhang, X. Huang, J.-S. Chen and X. Zou, *Nat. Commun.*, 2018, **9**, 5236
110. Y. Lu, W. Wang and F. Xie, *Mater. Res. Express*, 2019, **6**, (11), 115544
111. J. Yu, X. Wu, D. Guan, Z. Hu, S.-C. Weng, H. Sun, Y. Song, R. Ran, W. Zhou, M. Ni and Z. Shao, *Chem. Mater.*, 2020, **32**, (11), 4509
112. L. Zhang, H. Jang, Z. Li, H. Liu, M. G. Kim, X. Liu and J. Cho, *Chem. Eng. J.*, 2021, **419**, 129604
113. N. Li, L. Cai, C. Wang, Y. Lin, J. Huang, H. Sheng, H. Pan, W. Zhang, Q. Ji, H. Duan, W. Hu, W. Zhang, F. Hu, H. Tan, Z. Sun, B. Song, S. Jin and W. Yan, *J. Am. Chem. Soc.*, 2021, **143**, (43), 18001
114. Q. Zhang, X. Liang, H. Chen, W. Yan, L. Shi, Y. Liu, J. Li and X. Zou, *Chem. Mater.*, 2020, **32**, (9), 3904
115. R. Gao, Q. Zhang, H. Chen, X. Chu, G.-D. Li and X. Zou, *J. Energy Chem.*, 2020, **47**, 291
116. W. Sun, Y. Song, X.-Q. Gong, L. Cao and J. Yang, *ACS Appl. Mater. Interfaces*, 2016, **8**, (1), 820
117. W. Sun, L.-M. Cao and J. Yang, *Electrochim. Acta*, 2018, **260**, 483
118. C. Yang, G. Rousse, K. L. Svane, P. E. Pearce, A. M. Abakumov, M. Deschamps, G. Cibin, A. V. Chadwick, D. A. D. Corte, H. Anton Hansen, T. Vegge, J.-M. Tarascon and A. Grimaud, *Nat. Commun.*, 2020, **11**, 1378
119. W. Q. Zaman, W. Sun, M. Tariq, Z. Zhou, U. Farooq, Z. Abbas, L. Cao and J. Yang, *Appl. Catal. B: Environ.*, 2019, **244**, 295
120. J. Gao, X. Huang, W. Cai, Q. Wang, C. Jia and B. Liu, *ACS Appl. Mater. Interfaces*, 2020, **12**, (23), 25991
121. H. Li, H. Liu, Q. Qin and X. Liu, *Inorg. Chem. Front.*, 2022, **9**, (4), 702
122. D. R. Modeshia and R. I. Walton, *Chem. Soc. Rev.*, 2010, **39**, (11), 4303
123. R. J. Darton, S. S. Turner, J. Sloan, M. R. Lees and R. I. Walton, *Cryst. Growth Des.*, 2010, **10**, (8), 3819
124. K. Sardar, J. Fisher, D. Thompsett, M. R. Lees, G. J. Clarkson, J. Sloan, R. J. Kashtiban and R. I. Walton, *Chem. Sci.*, 2011, **2**, (8), 1573
125. C.-L. Ma, Z.-Q. Wang, W. Sun, L.-M. Cao, X.-Q. Gong and J. Yang, *ACS Appl. Mater. Interfaces*, 2021, **13**, (25), 29654
126. J. A. Clayton and R. I. Walton, *Johnson Matthey Technol. Rev.*, 2022, **66**, (4), 406-417

The Authors

Jasmine Clayton studied Chemistry at the University of Warwick, UK, graduating with MChem (Hons) in 2019. As a Masters student she undertook an international placement at the University of Modena and Reggio Emilia, Italy, under the supervision of Alfonso Zambon. Her final year research project on gallium substituted AlPO zeotypes was under the supervision of Professor Richard Walton. She is presently undertaking research for a PhD in collaboration with Johnson Matthey on acid-resilient OER catalysts and catalyst supports.

Richard Walton is Professor of Chemistry at the University of Warwick, and director of Warwick's X-ray facility. His research group investigate the synthesis and structures of inorganic materials, particularly from solution-based crystallisation, such as hydrothermal chemistry. This includes open-framework zeotypes and MOFs, as well as condensed oxide structures, that may have practical applications in areas related to energy and heterogeneous catalysis. He has collaborated with various scientists at Johnson Matthey for the past 20 years, and was Royal Society Industry Fellow from 2015–2019 at Johnson Matthey.